International Journal of Coal Geology 198 (2018) 63–76

Contents lists available at ScienceDirect

International Journal of Coal Geology

journal homepage: www.elsevier.com/locate/coal

Density and biomechanical properties of fossil fronds. A case study of *Neuropteris ovata* (seed fern, Late Pennsylvanian, Canada)

José A. D'Angelo[a,b,*], Erwin L. Zodrow[b]

[a] IANIGLA-CONICET, FCEN, Universidad Nacional de Cuyo, M5502JMA Mendoza, Argentina
[b] Palaeobotanical Laboratory, Cape Breton University, 1250 Grand Lake Rd., Sydney, Nova Scotia B1P 6L2, Canada

ARTICLE INFO

Keywords:
Medullosales
Neuropteris ovata
3D density model
FTIR
Biomechanics
Theoretical life habits
Autecology

ABSTRACT

A theoretical biomechanical model is proposed for the largest known 650 mm-long frond segment *Neuropteris ovata* var. *simonii* (Medullosales, Pennsylvanian, Sydney Coalfield, Canada). The study procedure includes, amongst others, a novel methodology for calculating density of fossil pinnules and rachides. This, in conjunction with the trait relationships and mathematical models that linked density and material/structural properties established for modern plant-leaf tissues, permits the estimation of tensile strength, tensile modulus of elasticity, flexural stiffness, and leaf mass per area. Results suggest that, theoretically, (a) the living frond invested a considerable amount of resources for the construction of metabolically expensive, hard, tough, and resistant pinnule and rachial tissues, which were "made to last", and (b) were used as part of a combination of strategies that increased the plant's biomechanical stability. This translated in resistance to damage during the application of external loads such as those exerted by strong winds or tropical storms. High leaf mass per area (dry-mass investment) of pinnules and rachial tissues points to a slow photosynthetic return that was sustained for long periods of time (long leaf lifespan). The latter possibly indicates a plant adaptation to wet, levee-top habitats, which were characterized by nutrient-deficient soils exposed to intensive solar irradiation. The 3D, chemistry-based model of the *N. ovata* specimen provided new insights into the hitherto poorly-known biomechanical and related traits of this iconic medullosalean plant that inhabited Pennsylvanian wetlands. Other implications of using our chemistry-based methodology include the estimation of (i) frond size and shape (plant reconstructions), (ii) plant ecophysiological adaptations to different wetland environments, and (iii) plant phylogenetic and ontogenetic adaptations.

1. Introduction

Arborescent seed ferns (Order Medullosales) from the Carboniferous were routinely depicted as being 10 m or taller (e.g., Pfefferkorn et al., 1984; Wnuk and Pfefferkorn, 1984) with a slender-trunk diameter of 20–25 cm, having an adventitious root system, and an impressively large crown consisting of a number of large, compound leaves (termed fronds). Most medullosalean fronds were possibly 1–2 m in length, although a considerably large *Alethopteris* specimen with a width of at least 2 m, and approximately 6 m long has been recorded by Laveine (1986). Medullosalean fronds generally had a robust construction with a bifurcation at the base, and were several times divided. In many cases, the last frond division, the pinnules, were thick and coriaceous, and could be as long as 6–7 cm (e.g., *Macroneuropteris scheuchzeri*; see Laveine and Belhis, 2007; see also Beeler, 1983).

The living habitat was diverse and could be in the developing coal swamp, or on drier parts. However, several detailed studies on *Medullosa* (i.e., the fossil genus assigned to the trunk of Medullosales) have suggested that these seed-bearing plants very likely had intolerance to water deficits (Wilson, 2013; Wilson et al., 2008, 2015, 2017). In addition to the general largeness of these seed ferns, they also bore seeds that were as large as 12 cm and probably represent the largest ovular category for the Carboniferous. Ovular attachment is assumed to a frond rather than the upper trunk.

Fossil remains of this plant-fossil group are very abundant, though fragmentary, occurring mostly as ultimate-pinna tips.

There are a few biomechanical studies of Paleozoic pteridosperms, which are only referred to trunks or large branches/stems (e.g., Rowe et al., 1993; Masselter et al., 2007). To the best of our knowledge, nothing has been published regarding the biomechanics of medullosalean rachides and pinnules. This paper investigates the biomechanical "strength" of these seed-fern trees, in order to understand how they

* Corresponding author at: IANIGLA-CONICET, FCEN, Universidad Nacional de Cuyo, M5502JMA Mendoza, Argentina.
E-mail addresses: joseadangelo@yahoo.com, jdangelo@uncu.edu.ar (J.A. D'Angelo).

https://doi.org/10.1016/j.coal.2018.09.003
Received 21 June 2018; Received in revised form 31 August 2018; Accepted 2 September 2018
Available online 04 September 2018

could survive storm-swept coal swamps. Used as a test case is the 650 mm *N. ovata* frond and its chemical composition, i.e., semi-quantitative data obtained by Fourier Transform infrared (FTIR) spectroscopy analysis. These FTIR data were previously published (D'Angelo and Zodrow, 2016 and Zodrow et al., 2017) and are used here to derive a new, multivariate model using principal component analysis (PCA). From this PCA model, estimates of biomechanical properties of strength, flexibility, bending, and support biomass distribution were calculated. This, however, presupposes the application of a newly developed methodological approach to derive data of fossil densities from the functional groups of the *N. ovata* frond. In effect, this is an introduction to the methodological analysis of theoretical life models of seed ferns. At the same time, this paper represents an alternative and complementary method to the reconstruction of seed ferns from purely macrofloral fragments, with unexpected information and biomechanical implications. It also illustrates an instance in which chemical data from a compression-plant fossil is fundamental for advancing basic research with direct implications for taxonomy and paleoecophysiology.

2. Note on biomechanical terminology

Standard biomechanical terminology focuses on defining mechanical properties of bending and flexure, and on how living-plant tissues cope with natural forces such as gravity (self-loading), wind (drag), and rain (e.g., Niklas and Spatz, 2010; Méndez-Alonzo et al., 2013; Gibson, 2012). We assume that applies to plant fossils as well.

The overall mechanical properties of biological composites depend on the material composition and the dimension and shape of the object (e.g., Onoda et al., 2011). Measured leaf mechanical properties are usually based on tensile tests (e.g., Balsamo et al., 2006), including material properties (tensile modulus of elasticity) and structural properties (tensile strength, and flexural stiffness):

(i) Tensile modulus of elasticity (in MPa = MN/m^2) is a measure of the intrinsic resistance of the leaf tissue to elastic deformation, i.e., the stiffness of the leaf tissue. The higher the tensile modulus of elasticity value, the stiffer the tissue. According to the International System of Units, 1 MPa = 1 megapascal = 1,000,000 Pascal (Pa, unit for pressure) and 1 MN = 1 meganewton = 1,000,000 Newton (N, unit of force).

(ii) Tensile strength (in MPa) is the force required to fracture the leaf per unit of sectional area.

(iii) Flexural stiffness (in Nm^2) measures the total structural resistance to bending, representing the tensile modulus of elasticity normalized by the structure dimensions. Under a given load, the larger the flexural stiffness value, the smaller the energy absorbed by the tissue and the smaller the deformation (e.g., Vogel, 2003). Flexural stiffness (FS) is the product of the tensile modulus of elasticity (TME) of the plant part and the second moment of area (I_0), i.e., FS = TME x I_0. The second moment of area is a property of the cross-sectional geometry of an object, and describes the mass distribution around a given center of mass. Niklas (1992) mathematically derived some formulae for the calculation of the second moment of area for objects with standard geometric shapes. We considered that the cross sections of different order rachides were circular and the second moment of area was calculated as $I_0 = (\pi/64)\ D^4$; where D is the diameter of the transverse axis (rachis). More details on the derivation of the equation can be found in Niklas (1992, p.136, Fig. 3.3). During fossilization frond parts deform under pressure and rachis-diameter changes occur. However, as experimentally demonstrated by Rex and Chaloner (1983), deformation in diameter is generally minimal in compression-impression specimens. Thus, in this study the diameter of the fossil specimens was directly measured while still embedded on the rock matrix, which possibly implies uniformly (though slightly) overestimated flexural-stiffness values.

Mechanical resistance of leaves described by the material and structural properties mentioned above (i - iii) are also related to the leaf dry mass per unit area (hereafter termed leaf mass per area; g/cm^2), which represents the leaf dry-mass investment per unit of light-intercepting leaf area deployed. Since leaf mass per area is one of the easy to measure parameters in living plants, it is considered, and frequently used, as a good predictor of plant performance (e.g., Wright et al., 2004). Leaf mass per area is an important measure of the biomass allocation (carbon storage) to leaf tissues (e.g., Bazzaz and Grace, 1997) and correlates positively with their density, thickness, and material structural resistance (e.g., Wright et al., 2004). Furthermore, it is well known that species with high leaf mass per area have a denser tissue or thicker leaf blade (or both), and higher tensile strength, tensile modulus of elasticity, and flexural stiffness (e.g., Onoda et al., 2011). Leaf mass per area is considered an important indicator for the distribution of the support biomass, i.e., the partitioning of structural resistance of leaf tissues, which contributes to maintaining the mechanical stability of fronds.

3. Materials, methods, and quantitative data

3.1. N. ovata frond 85-248

The study specimen was collected from the basal Cantabrian strata in the Sydney Coalfield of Nova Scotia, or 3.5 m above the Point Aconi coal Seam (Fig. 1). The taxonomic history of the study specimen (Fig. 2) is summarized as *Neuropteris ovata* (Hoffmann, 1826) var. *simonii* (Bertrand, 1930) Zodrow and Cleal, 1988, hereafter called *ovata* frond, or *ovata* plant.

On the basis of vitrinite reflectance (R_o%) values of 0.79% for the Point Aconi Seam, we inferred that minimal diagenetic alterations or milder fossilization conditions prevailed (Zodrow et al., 2009).

Details regarding the methods, particularly the semi-quantitative FTIR analysis used, can be found in the Appendix (supplementary data), which includes the following information: Table 1: main functional groups and classes of compounds; and Table 2: definition of semi-quantitative area ratios derived from FTIR spectra.

3.2. Statistical methods

PCA was used to reduce the dimensionality of the data matrix to evolve a parsimonious set of groupings (e.g., Izenman, 2008), and to evaluate it as a function of IR-derived groups or chemical structures (e.g., D'Angelo et al., 2012; D'Angelo and Zodrow, 2015, 2016). We retained the number of components whose explained cumulative variance was at least 80% (Tables 3 to 5 of the Appendix; supplementary data).

Analysis of variance (ANOVA) is a statistical technique that can be used to compare means (groups or variables) of two or more sample sets using the F- distribution (Fisher, 1970). The null hypothesis poses that the means of all selected datasets are equal. Underlying assumptions include (i) normal distribution though appreciable deviation from normality is not a problem because of robustness (Donaldson, 1966), (ii) homoscedasticity, and (iii) independence of variables. We tested the calculated principal components and their estimated morphological and biomechanical properties.

3.3. Group-contribution method and density calculation

In chemistry, a group-contribution method is a technique to calculate and predict thermodynamic and other properties of both pure components and mixtures, using well-known properties of atoms, functional groups, and molecules (e.g., Constantinou and Gani, 1994; Jankowski et al., 2008). Property calculations by means of group-

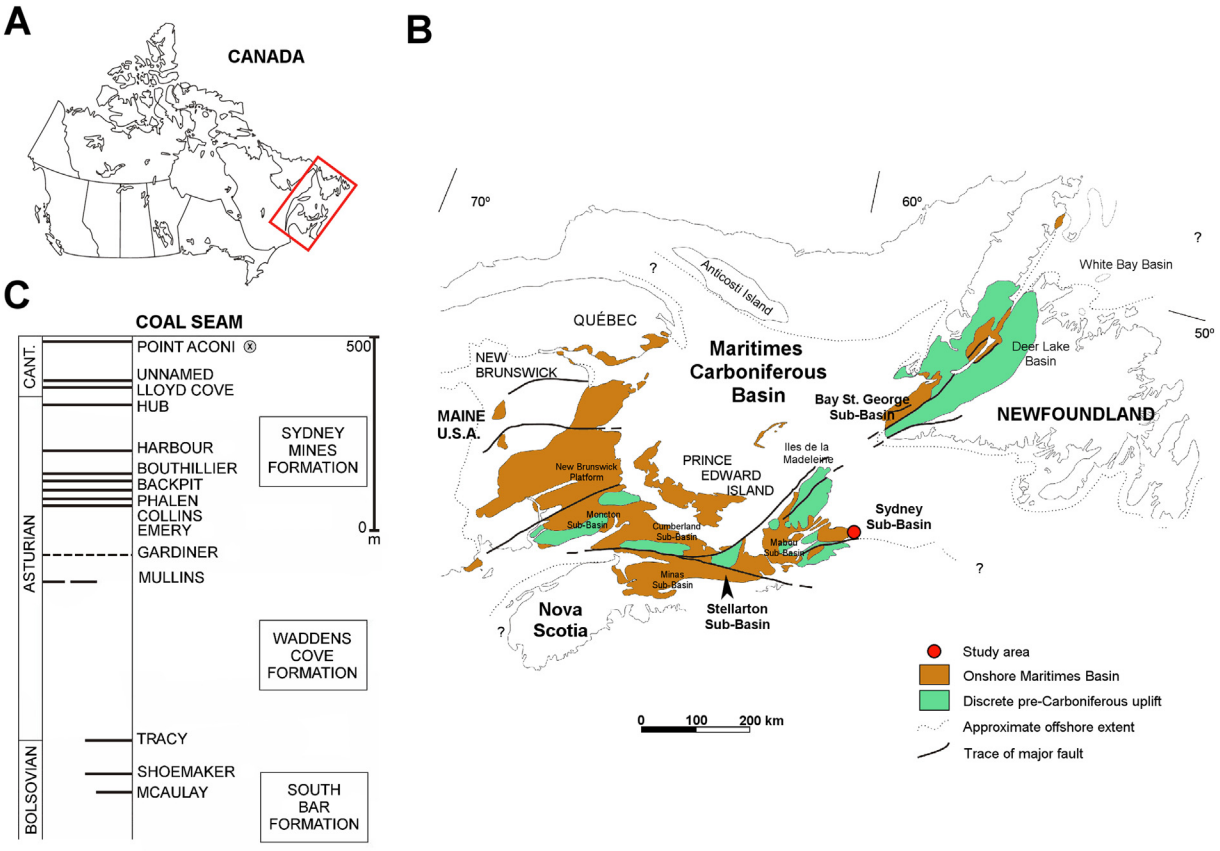

Fig. 1. Study location. (A) Canada. (B) Maritimes Basin with Sydney Coalfield (Sub-Basin), Nova Scotia. (C) Local coal stratigraphy. Sampled crevasse-splay (X) above the Point Aconi Seam (basal Cantabrian = CANT., see Zodrow and Cleal, 1985, Fig. 5; Zodrow and Cleal, 1988, Text-Figs. 1 to 4).

contribution methods are based on the assumption that the properties of pure components and mixtures can be calculated using additive atomic and group increments. These methods are useful for obtaining reliable estimates of macroscopic properties that include molecular weight, molar volume, surface tension, and density which are difficult to obtain by experimental measurements.

Using algorithms of ACD/ChemSketch (2010), Freeware version 12.01; www.acdlabs.com), we calculated two basic (as opposed to being derived) macroscopic properties that are molecular weight and molar volume for some proposed molecular structures, hypothetically present in the geomacropolymers constituting different parts of the frond specimen. Proposed molecular structures were based on both (i) data from the literature and (ii) the relative proportions of functional groups found in the *ovata* frond. The additive-constitutive atomic increments for molecular weight and molar volume are a function of the single, double, and aromatic chemical bond types between the atoms considered, and are based on a large experimental database (e.g., Constantinou and Gani, 1994; Jankowski et al., 2008). Values of molecular weight and molar volume were used to calculate density (molecular weight/molar volume).

3.4. Surface-fitting procedure

Our proposed molecular structures, hypothetically present in the different parts of the frond specimens were plotted as PC 1, PC 2, and PC 3 scores, their positions in the plot being approximate according to their relative contents of functional groups. Using a distance-weighted least squares procedure (McLain, 1974), a surface function was fitted to the complete data set consisting of fossils, coals, and proposed molecular structures. The data set was useful to reveal hidden patterns and to detect relationships amongst the three variables (PC 1, PC 2, and PC 3) in the plot (Zhou and Han, 2008). The projected contours of the fitted surface can be seen on the PC 1 – PC 2 component plane. Unlike some other weighted least squares fitting methods (see Atieg and Watson, 2003), in this procedure the surface function cannot be easily described by a single formula and is plotted independently from the data (see D'Angelo and Zodrow, 2011).

4. New methodology for density: Biomechanical implications

Using a helium pycnometer, density measurement is a cumbersome procedure, which requires relatively high sample weights (at least 1 g) for an accurate individual determination (Viana et al., 2002). Accurate density measurements of pinnules and rachides therefore are almost impossible to perform because sufficient sample sizes cannot be obtained. Alternatively, we present a novel methodology for obtaining density values of the different frond parts, which, in turn, were employed to estimate the biomechanical properties of tensile modulus of elasticity, tensile strength, flexural stiffness, and leaf mass per area. Present results help to better understand the poorly-known relationship amongst chemical (molecular) structure, morphological / architectural structure, and biomechanical characteristics of large medullosalean compound leaves, exemplified by the *ovata* frond.

The flow diagram shown in Fig. 3 summarizes steps (1) to (5):

(1) Samples are analyzed by semi-quantitative FTIR and data are evaluated by PCA. Loading plots indicated which combinations of functional groups were associated with which sample.
(2) Different combinations of specific functional groups in (1) allowed proposing some chemical moieties, hereafter termed standards. Then, specific standards can be associated with specific samples.
(3) Using a group-contribution method, density values can be

Fig. 2. Studied specimen. *Neuropteris ovata* var. *simonii* (specimen 85–248).

calculated for standards proposed in (2).

(4) Proposed standards, and their corresponding density values, are associated with samples. A surface-fitting procedure and a simplified mathematical model based on the relationship between samples IR-derived ratios and density values of standards are obtained. Hence, different parts of a fossil frond could be assigned approximate density values.

(5) Using linear regression analysis along with well-known relationships between chemical composition and some mechanical properties of living plants, pinnules and rachides can be assigned approximate values of biomechanical properties.

Steps (1) to (5) are explained in detail in the following sections.

4.1. Component loadings and standards

Considering the functional-group information provided by component-loading plots (step (1) of Fig. 3), we proposed several standards, representing possible, simple molecular structures of the geomacromolecules of the coalified parts of the *ovata* frond (step (2) of Fig. 3).

Component-loading plots provided detailed information about which combination of functional groups (IR-derived ratios) is most-closely associated with which sample. At the same time, these plots indicated which combination of functional groups is most associated with specific standards. Such information is indispensable because individual compounds (and their molecular structures) are unknown for complex, organic, multi-component samples (e.g., van Bergen et al., 2004), which is the case of the organic components recovered from the *ovata* frond.

Important to note is that our proposed standards are in general agreement with the apparent, relative proportions of functional groups shown by some molecular models suggested for common polymers found in fossil plants, coals, kerogens, and related, organic, sedimentary materials (e.g., Hatcher, 1990; van Bergen et al., 2004; Petersen et al., 2008; Zodrow et al., 2009; Heredia-Guerrero et al., 2014). This is the case of terpenoid- or partially aromatized terpenoid-like structures occurring in the interpenetrating polymeric networks reported from diagenetically modified resins, tannins, and lignin structures, as well as from some coals (e.g., Hatcher, 1990; Petersen et al., 2008; Heitner et al., 2010; D'Angelo and Zodrow, 2016; and many others). In fact, the presence of ether, carbon-carbon and carbonyl bridges, along with hydroxyl, aromatic carbon bonds, and some other functional groups, assures appropriate structural models for the geomacropolymers regarding their structural flexibility and thermodynamic stability (e.g., Shinn, 1984).

4.2. Proposed standards

Considering positive and negative component loadings on the eleven IR-derived ratios, the positions of 62 representative standards were proposed on the PC 1 – PC 2 and PC 1 – PC 3 component planes (Fig. 4A, B). The relative positions are shown in Fig. 4C.

A list of the proposed standards and their associated combination of functional groups are compiled in Table 6 of the Appendix (supplementary data). In general terms, standards include aliphatic and aromatic hydrocarbons with numerous combinations of different functional groups as revealed by the loadings plots.

Some suggested standards (structures # 1-27 and # 51-62; Table 6, Appendix; supplementary data) have straight polymethylenic chains of variable lengths and branching degrees as indicated by the recorded IR-derived ratios CH_2/CH_3, CH_{al}/Ox, $CH_{al}/C=C$, and 'A' factor. Non-straight-chain aliphatics such as naphthenic structures were proposed as well. Other suggested standards have variable contents of oxygen-bearing functional groups: C=O/C=C, C=O cont, $CH_{al}/C=O$, and 'C' factor.

A number of aromatic-rich standards (structures # 28–50) were proposed according to their relative contents of C=C cont, CH_{ar}/CH_{al}, $CH_{ar}/C=C$. Suggested aromatic structures have variable values of both aromaticity and condensation degree of aromatic nuclei (polycyclic rings). As an example, IR-derived ratios determined for pinnules and antepenultimate rachides samples are better described by aromatic compounds having variable aromaticity and condensation degree of benzene rings (standards # 28–50), whereas ultimate rachides can better be characterized by mainly aliphatic-containing compounds (standards # 15–28) (Table 6 of the Appendix; supplementary data).

4.3. Proposed standards and density

Using a group-contribution method, density values could be calculated for proposed standards (step (3) of Fig. 3). By means of calculated densities, samples could be assigned approximate density values. Thus, for example, specimens *2Pi*, *3Pi*, *4Pi*, *5Pi*, *6Pi*, *24APUr*, *26APUr*, and *28APUr* (specimen identification followed Fig. 2 of D'Angelo and Zodrow, 2016) were associated with proposed standard # 43 (see Fig. 4D–F and Tables 6 and 7 of the Appendix; supplementary data) with a calculated density of 1.19 g/cm^3.

Important to note is that minor changes introduced in the proposed functional-group types of the different standards yielded relatively small differences (ca. 10%) in their corresponding density values (Figs. 1 and 2 of the Appendix, supplementary data). Implied is that the proposed standards did not need to be the "exact combination" (if there is any) of functional groups. For example, the difference in density values between standards (a) # 1 and # 2 is 5.2%; (b) # 22 and # 23 is

Table 1
Estimated values of density (δ), tensile strength (TS), tensile modulus of elasticity (TME), diameter (D), flexural stiffness (FS), and leaf mass per area (LMA) for *N. ovata*. Diameter and flexural stiffness were estimated only for the frond support units i.e., rachides of different orders.

#	Specimen identification [a]	Sample Type [b]	δ (g/cm^3)	TS (MPa)	TME (MPa)	D (m)	FS (Nm^2)	LMA (g/cm^2)
1	*1Pi*	FC	0.94	3.87	502.6	n. d.	n. d.	0.70
2	*2Pi*	Comp	1.19	7.26	2577.3	n. d.	n. d.	0.93
3	*3Pi*	Comp	1.19	7.26	2577.3	n. d.	n. d.	0.93
4	*4Pi*	Comp	1.19	7.26	2577.3	n. d.	n. d.	0.93
5	*5Pi*	Comp	1.19	7.26	2577.3	n. d.	n. d.	0.93
6	*6Pi*	Comp	1.19	7.26	2577.3	n. d.	n. d.	0.93
7	*7Pi*	Comp	1.01	4.58	779.4	n. d.	n. d.	0.77
8	*8Pi*	Comp	1.01	4.58	779.4	n. d.	n. d.	0.77
9	*9Pi*	Comp	1.01	4.58	779.4	n. d.	n. d.	0.77
10	*10Pi*	Comp	0.92	3.63	425.8	n. d.	n. d.	0.68
11	*11Pi*	Comp	0.98	4.22	628.9	n. d.	n. d.	0.74
12	*12Pin*	Comp	1.01	4.58	779.4	n. d.	n. d.	0.77
13	*13Ur*	FC	0.88	3.35	345.8	7.7×10^{-4}	5.9×10^{-6}	0.65
14	*14Ur*	Comp	0.99	4.38	694.5	7.7×10^{-4}	1.2×10^{-5}	0.75
15	*15Ur*	Comp	0.99	4.38	694.5	7.7×10^{-4}	1.2×10^{-5}	0.75
16	*16PUr*	FC	0.88	3.35	345.8	0.004	0.005	0.65
17	*17PUr*	Comp	0.96	4.06	568.6	0.004	0.009	0.72
18	*18PUr*	Comp	0.98	4.22	628.9	0.004	0.007	0.74
19	*19PUr*	Comp	1.00	4.54	759.4	0.004	0.008	0.76
20	*20PUr*	Comp	0.92	3.63	425.8	0.003	0.002	0.68
21	*21PUr*	Comp	0.94	3.85	496.1	0.003	0.002	0.70
22	*22APUr*	FC	0.88	3.35	345.8	0.011	0.228	0.65
23	*23APUr*	Comp	1.18	7.00	2345.5 [c]	0.011	1.549	0.92
24	*24APUr*	Comp	1.19	7.26	2577.3 [c]	0.011	1.702	0.93
25	*25APUr*	Comp	0.92	3.63	425.8	0.005	0.013	0.68
26	*26APUr*	Comp	1.19	7.26	2577.3 [c]	0.005	0.079	0.93
27	*27APUr*	Comp	0.92	3.63	425.8	0.005	0.013	0.68
28	*28APUr*	Comp	1.19	7.26	2577.3 [c]	0.005	0.079	0.93

n. d. = not determined.
[a] See Fig. 2 of D'Angelo and Zodrow (2016) for specimens identification.
[b] Sample type: FC = fossilized-cuticle, Comp = compression.
[c] These values are similar to those reported for wood lignins (Gibson, 2012) i.e., 2500 to 3700 MPa.

2.1%; and (c) # 13 and # 26 is 2.8%. Hence, overall calculated density values obtained for our fossilized organic material are in general agreement with the scarce density data characterizing coalified compressions (see Boucher et al., 1999 for some estimated density data). In fact, experimentally determined values of compression densities are ca. 1.38 g/cm^3 (M. Mastalerz, personal communication, 2015). This value is similar to our calculated values, which were in the range 0.80 g/cm^3–1.20 g/cm^3 (mean value = 1.02 ± 0.09 g/cm^3).

4.4. Model of density zones

Our 62 standards were plotted in the 3D component-score plots and their relative positions are shown by Fig. 4D.

(i) A distance-weighted least squares procedure was used to fit a surface to the PC 1, PC 2, and PC 3 coordinate data (McLain, 1974; step (4) of Fig. 3). Fig. 4E shows the result of the surface (three-dimensional) plot with indication of standards and samples.

(ii) The fitted surface was projected on the plane defined by the two most important components, i.e., PC 1 – PC 2 (cumulative explained variance is 74.37%) (Fig. 4F). Projected contour colors represent approximate density zones, where different *ovata*-frond parts are associated with standard density values.

4.5. Simplified density model

The surface function and the plot of approximate density zones (Fig. 4E and F, respectively) cannot be easily described by a single formula and plotted independently from the data (see Atieg and Watson, 2003, and D'Angelo and Zodrow, 2011). In order to comply with a simple way to calculate density values, a simplified 3D model was derived, i.e., the "3D density model".

According to the solution of our PCA model (Tables 3 to 5 of the Appendix; supplementary data), PC 1 (57.47% explained variance) has the highest positive loading on CH_{ar}/CH_{al} and the highest negative loading on C = O/C = C. These two ratios represent the abundance of aromatic functionalities vs. aliphatic- and oxygen-containing functional groups, summarizing the overall characteristics of the proposed standards.

In an attempt to obtain an empirical relationship, linear regression analysis was performed on the dataset step (5) of Fig. 3), with density as the dependent variable and CH_{ar}/CH_{al} and C = O/C = C as assumed independent variables. The following equation was obtained (Fig. 5), where bracketed values are the standard errors of the estimate:

$$\delta = 0.94 - 1.86\ C = O/C = C + 0.45 CH_{ar}/CH_{al} \quad R^2 = 0.57$$
$$(0.03)\quad (0.43)\qquad\qquad (0.08)\qquad\qquad R = 0.76, \qquad (1)$$

where δ = density is in g/cm^3.

Table 7 of the Appendix (supplementary data) shows the density values obtained using both the 3D chemical map and a linear fit (Eq. (1)). One-way ANOVA indicated that with 95% confidence no significant differences existed between the density values obtained using both 3D chemical map and the linear fit Eq. (1) ($p > 0.05$, see Table 8, Appendix, supplementary data). This probably demonstrates the reliability of Eq. (1), which provides a simple way to calculate density values.

5. Results

5.1. Changes in molecular structures reflect frond morphology and architecture

Morphological studies on living vascular plants include the analysis

Table 2
Summary of morphological and biomechanical traits of different frond parts. Descriptive statistics: mean values of density (δ; g/cm^3), tensile strength (TS; MPa), tensile modulus of elasticity (TME; MPa), diameter (D; m), flexural stiffness (FS; Nm^2), and leaf mass per area (LMA; g/cm^2) for *N. ovata*. Diameter and flexural stiffness were estimated only for the frond support units i.e., rachides of different orders. Fossilized-cuticle samples were not considered.

Frond part/Variable	Mean	SD	Min	Max	*N*	Frond part/Variable	Mean	SD	Min	Max	*N*
Pi						Ultimate pinna [a]					
δ	1.09	0.11	0.92	1.19	11	δ	1.07	0.10	0.92	1.19	13
TS	5.68	1.45	3.63	7.26	11	TS	5.47	1.45	3.67	7.21	13
TME	1550.8	957.9	425.8	2577.3	11	TME	1402.7	930.1	437.1	2527.5	13
D	n. d.	n. d.	n. d.	n. d.	–	D	n. d.	n. d.	n. d.	n. d.	–
FS	n. d.	n. d.	n. d.	n. d.	–	FS	n. d.	n. d.	n. d.	n. d.	–
LMA	0.83	0.01	0.68	0.93	11	LMA	0.82	0.10	0.68	0.93	13
Ur						Penultimate pinna [b]					
δ	0.99	0	0.99	0.99	2	δ	1.04	0.10	0.92	1.19	18
TS	4.38	0	4.38	4.38	2	TS	5.08	1.39	3.67	7.21	18
TME	694.5	0	694.5	694.5	2	TME	1173.2	871.2	437.0	2527.5	18
D	8×10^{-4}	0	8×10^{-4}	8×10^{-4}	2	D	n. d.	n. d.	n. d.	n. d.	–
FS	1×10^{-5}	0	1×10^{-5}	1×10^{-5}	2	FS	n. d.	n. d.	n. d.	n. d.	–
LMA	0.75	0	0.75	0.75	2	LMA	0.79	0.09	0.68	0.93	18
PUr						Complete frond fragment [c]					
δ	0.96	0.03	0.92	1	5	δ	1.05	0.11	0.92	1.19	24
TS	4.06	0.32	3.63	4.54	5	TS	5.31	1.52	3.67	7.21	24
TME	575.8	118.0	425.8	759.4	5	TME	1331.0	939.9	437.0	2527.5	24
D	0.004	0.0005	0.003	0.004	5	D	n. d.	n. d.	n. d.	n. d.	–
FS	0.006	0.003	0.002	0.009	5	FS	n. d.	n. d.	n. d.	n. d.	–
LMA	0.72	0.03	0.69	0.76	5	LMA	0.81	0.10	0.68	0.93	24
APUr											
δ	1.10	0.14	0.92	1.19	6						
TS	6.01	1.80	3.63	7.26	6						
TME	1821.5	1060.8	425.8	2577.3	6						
D	0.007	0.003	0.005	0.011	6						
FS	0.57	0.82	0.013	1.70	6						
LMA	0.85	0.13	0.68	0.93	6						

n. d. = not determined.
[a] Mean values of *Pi* + *Ur*.
[b] Mean values of *Pi* + *Ur* + *PUr*.
[c] Mean values of *Pi* + *Ur* + *PUr* + *APUr*.

of their architecture, i.e., the nature and relative arrangement of their different parts (e.g., Hallé and Oldeman, 1970). The arrangement can be seen as a hierarchically branched system constituted of different axial categories, which have specific functions and structures (e.g., Barthélémy and Caraglio, 2007). Structurally, axes and leaves differ mainly in the characteristic distribution patterns of different tissues: epidermis, mesophyll, and vascular tissue, which depend on the plant part and plant taxon (cf. Evert, 2006). Different groupings of cells, characterized by several combinations of chemical compounds, can be found according to their position and function in the plant body. Because of the close relationships amongst the individual compounds, small changes in cell-wall chemistry can considerably affect their structure and functioning ability (e.g., Niklas, 2004). Although with some limitations (e.g., deformation by compaction and fragmentary nature of fossil remains), some morphological and architectural studies can be carried out on different parts of fossil plants, particularly the leaf, which is the most frequently preserved plant structure.

Based on some anatomical studies of permineralized Medullosales (e.g., Beeler, 1983), and in a manner similar to living plants, we consider that a morphological and anatomical continuity existed throughout a fossil frond. Thus, produced was a continuum of variation of characteristics from the cell/tissue scale, to the anatomical organization, to the gross morphology and architecture. The *ovata* frond is characterized by a number of hierarchical categories of axes of tri- or quadripinnate (?) degree of segmentation, and provides a good opportunity to (chemically) study its architecture. Here, we demonstrate the anatomical and morphological continuities of different, original tissues in the *ovata* frond revealed by their chemical composition, including the geometry of the molecular structure (functional groups).

5.2. Chemical differences amongst pinnules and rachides of different order

Although IR spectra indicate that some functional groups are similar in certain parts of the *ovata* frond, our chemometric model emphasizes the relatively different ratios of chemical groups useful to distinguish (a) pinnules from rachides, and (b) rachides of different orders. These results are in agreement with the few, semi-quantitative, IR-derived data published so far (e.g., Zodrow and Mastalerz, 2002; D'Angelo and Zodrow, 2016; D'Angelo et al., 2011).

Pinnules of the *ovata* frond exhibited relatively lower amounts of aliphatics with shorter polymethylenic side chains, and higher contents of aromatics than rachides. The recorded order of aromaticity is: pinnule ≈ antepenultimate rachis > penultimate rachis > ultimate rachis. With 95% confidence, and considering PC 1 data as a proxy for the chemical composition, one-way ANOVA revealed significant differences ($p < 0.05$; Table 9, Appendix, supplementary data) between pinnules and ultimate rachides as well as between pinnules and penultimate rachides.

PC 1 data for pinnules and antepenultimate rachides were not significantly different. Such a result is explained by the similar contents of aromatic functional groups found in both pinnules and antepenultimate rachides. However, the type of aromatic compounds was possibly different in the two frond parts. Higher contents of tannin-related structures were present in pinnules, whereas higher contributions of lignin-like compounds were more frequent in antepenultimate rachides (see D'Angelo and Zodrow, 2016).

As expected and considering PC 1 data, one-way ANOVA showed significant differences amongst ultimate rachides, penultimate rachides, and antepenultimate rachides. This result confirms the utility of our chemometric model to chemically discriminate pinnules from rachides and to identify the order of rachides.

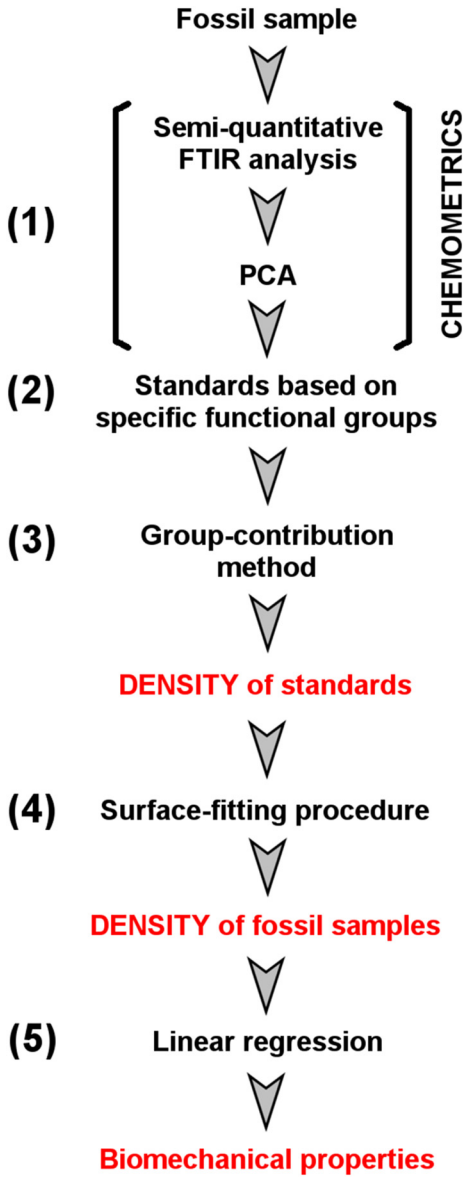

Fig. 3. Flow diagram showing the main steps involved in the development of the new methodology for obtaining density and biomechanical properties of fossil frond parts.

The complete set of one-way ANOVA comparisons involving the three PCs and different plant parts combinations can be found in Table 9 of the Appendix (supplementary data).

5.3. Chemical differences amongst proximal and distal frond parts

An arbitrary division of the frond into proximal and distal parts permitted more detailed chemical comparisons using one-way ANOVA tests. The proximal part of the frond included: *2Pi*, *3Pi*, *4Pi*, *5Pi*, *6Pi*, *14Ur*, *18PUr*, *19PUr*, *23APUr*, *24APUr*, and *25APUr*, whereas the distal frond part included: *7Pi*, *8Pi*, *9Pi*, *10Pi*, *11Pi*, *12Pin*, *15Ur*, *17PUr*, *20PUr*, *21PUr*, *26APUr*, *27APUr*, and *28APUr* (see Table 7, Appendix, supplementary data and Fig. 2 of D'Angelo and Zodrow, 2016 for specimen identification).

Statistically, chemical distinctions could be made between data representing proximal and distal pinnules. The distinctions between proximal and distal penultimate rachides, and between proximal and distal antepenultimate rachides were possible as well. Statistical differentiation between proximal and distal ultimate rachides could not be calculated because of limited sample supply.

With 95% confidence, one-way ANOVA indicated that PC 1 data obtained for the proximal pinnules (*1Pi* to *6Pi*) were significantly different from those of the distal ones (*7Pi* to *11Pi*) (Tables 7 and 10, Appendix, supplementary data). In fact, proximal pinnules showed a relatively more aromatic composition (higher values of CH_{ar}/CH_{al}) and higher condensation degrees (higher values of $CH_{ar}/C=C$) than distal pinnules. On the other hand, distal pinnules showed a relatively higher values of aliphatics (e.g., higher $CH_{al}/C=C$ and 'A' factor ratios). Relatively high C=O contents (lower values of $CH_{al}/C=O$) recorded for *11Pi* indicated likely ester bridges, i.e., a higher cross-linking degree. It is noted that the only intercalary pinnule (*12Pin*) analyzed could not be differentiated from the rest of the distal pinnules.

Considering PC 1 data, one-way ANOVA comparisons ($\alpha = 0.05$) indicated no significant differences ($p > 0.05$; Table 10, Appendix, supplementary data) between proximal (*17PUr*, *20PUr*, *21PUr*) and distal (*18PUr* and*19PUr*) penultimate rachides. However, slightly higher aromaticity and condensation degrees of the aromatic rings were recorded for proximal penultimate rachides, whereas distal penultimate rachides showed slightly higher values of oxygen- and aliphatic-bearing compounds.

Similarly, considering PC 1 data, one-way ANOVA indicated that proximal (*23APUr* to *25APUr*) antepenultimate rachides were not significantly different from distal (*26APUr* to *28APUr*) ones. However, noted is that proximal parts of the antepenultimate rachides showed a rather poor aliphatic composition (the lowest values of $CH_{al}/C=C$) as well as slightly higher aromatic contents than distal sections of the antepenultimate rachides.

5.4. 3D chemical maps and the biomechanics of the ovata frond

In this section, the relationship between variability of chemical composition and some mechanical properties will be addressed, emphasizing at the same time the analysis of the biomechanical stability of the different parts of the *ovata* frond.

5.4.1. Plant biomechanics

Plant biomechanics is the study of the structure and function of organs and tissues by means of mechanics, including structural analyses and strength of materials (e.g., Niklas, 1992; Boudaoud, 2010). Studies on evolutionary biomechanical adaptations and inferences on extinct plant biomechanical functions are possible from paleobotanical remains (e.g., Niklas and Kutschera, 2009), provided organic remains are preserved (e.g., D'Angelo and Zodrow, 2016).

5.4.2. Estimation of the biomechanical traits of leaves

Extant plant materials are made up of different tissues, which can be simple (made up of a single cellular type) or complex (constituted by different cellular types), each having their own structures (Evert, 2006). Experimental determinations of biomechanical properties of leaves, stems, and roots are performed employing different testing methods, including the use of several mechanical instruments such as tensometers, screw side-action grips, and penetrometers (Niklas, 1992). Evaluations of biomechanical properties of plant materials have been carried out mainly on wood and woody tissues: bark, trunk, and stems (Niklas and Spatz, 2010). Yet, quantitative data on biomechanical properties of leaves (at the tissue and whole-leaf scales) in extant plants are scarce (Onoda et al., 2011; Méndez-Alonzo et al., 2013).

In this contribution, density of different frond parts could be calibrated with the tensile modulus of elasticity, tensile strength, and leaf mass per area from published experimental data (Méndez-Alonzo et al., 2013). Those results indicated that the response of leaf density to leaf tensile modulus of elasticity and tensile strength were markedly nonlinear, whereas that of leaf density to leaf mass per area was linear. Experimental data from the literature were fitted using the following equations:

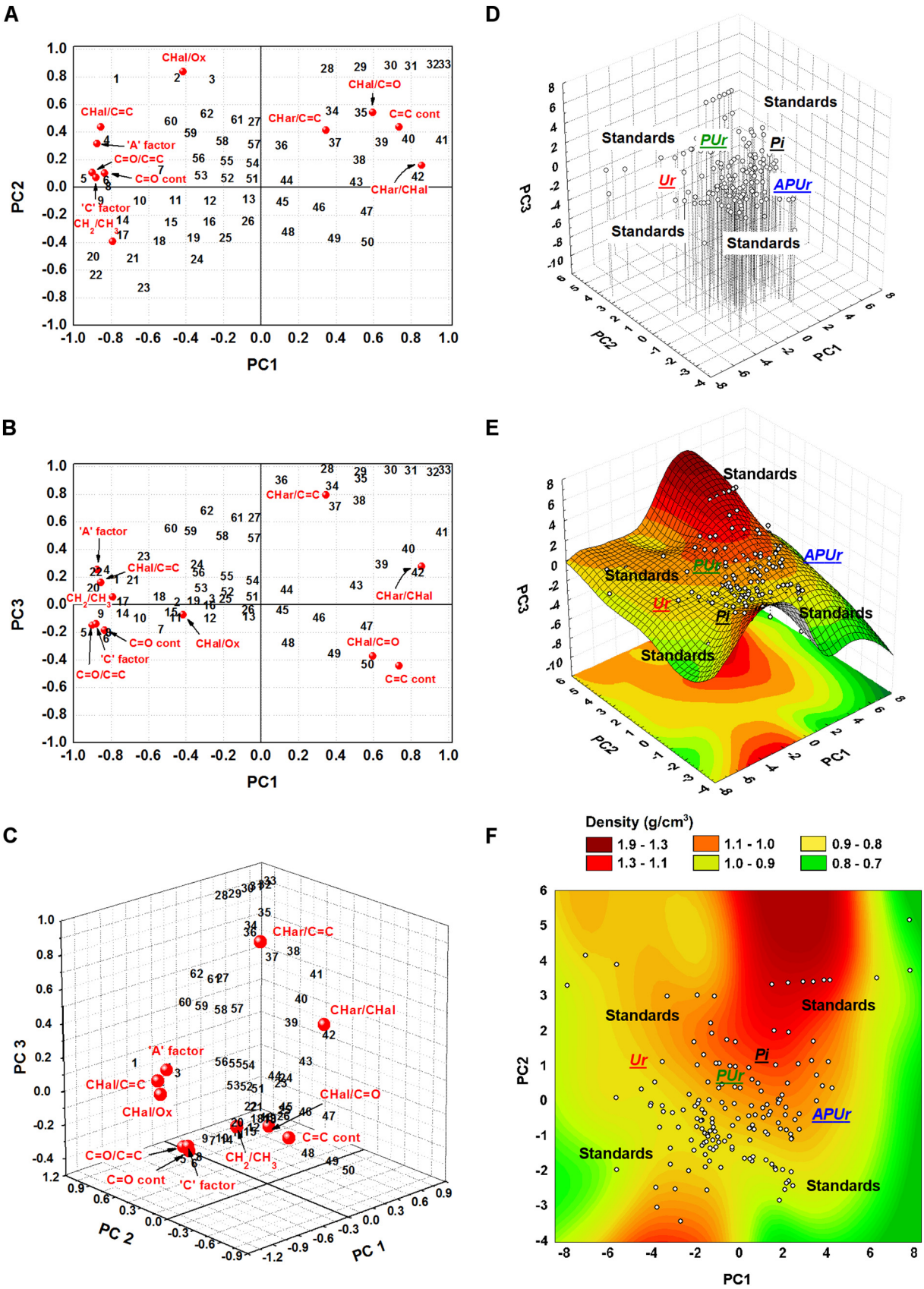

Fig. 4. Positions of 62 standards (i.e., combination of functional groups and IR-derived ratios) on the (A) PC 1 – PC 2 and (B) PC 1 – PC 3 component planes. (C) Relative positions of the 62 proposed standards in the 3D component loadings plot. (D) 3D component scores plot showing which standards is most associated with which sample i.e., frond parts. (E) Surface (three-dimensional) plot (sets of PC 1, PC 2, and PC 3 coordinates) with indication of standards and samples. (F) Projected contours of the fitted surface on the PC 1 - PC 2 component plane shown in (E) where colors represent approximate density zones. Density values were calculated considering the molecular structures of the proposed structural moieties (see text for details). Different frond parts are associated with approximate density values. For a better interpretation of the color references in this figure, the reader is referred to the web version of this article.

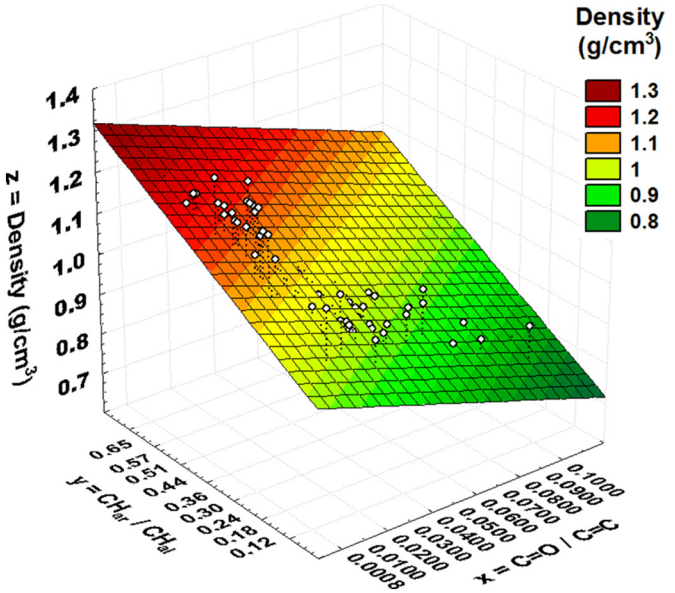

Fig. 5. 3D density model showing the interdependency amongst the three parameters: $\delta = 0.94–1.86C=O/C=C + 0.45\ CH_{ar}/CH_{al}$.

$$\ln(TME) = 6.50\,\delta + 0.10;\quad R^2 = 0.82$$
$$(0.02)\quad (0.01)\qquad R = 0.901 \tag{2}$$

$$ln\,(TS) = 2.50\,\delta - 1.0;\quad R^2 = 0.73$$
$$(0.02)\quad (0.1)\qquad R = 0.85 \tag{3}$$

$$LMA = (0.1 + (6.5\delta) - 1.3)/7;\quad R^2 = 0.61$$
$$(0.03)\ (0.02)\ \ (0.01)\qquad R = 0.78, \tag{4}$$

where δ = density (in g/cm^3), TME = tensile modulus of elasticity (in MPa), TS = tensile strength (in MPa), and LMA = leaf mas per area (in g/cm^2), and bracketed values are standard errors.

Eqs. (2), (3), and (4) were then used to estimate the tensile modulus of elasticity, tensile strength, and leaf mass per area from individual density values. They were obtained from experimental, FTIR-derived data, for the different parts of the *ovata* frond. Table 1 shows the calculated density values and the corresponding estimated values of the biomechanical properties relating to the study samples. Table 2 lists a summary (descriptive statistics) of morphological and biomechanical traits of the different frond parts.

Values of density, tensile strength, tensile modulus of elasticity, flexural stiffness, and leaf mass per area obtained for the fossilized pinnules, intercalary pinnule, ultimate rachides, penultimate rachides, antepenultimate rachides are in general agreement with measured values characterizing similar materials in living plants. This is the case of parenchyma and vascular bundles of extant plants, containing lignin and hemicellulose (see Gibson, 2012).

However, it should be recalled that the approximate values of tensile strength, tensile modulus of elasticity, flexural stiffness, and leaf mass per area obtained here represent preserved, geomacromolecular (i.e., NOT biomacromolecular) compounds of fossilized plants. As expected, taphonomically biased results were obtained and direct comparisons with living plant materials were not possible. However, and considering the favorable preservational conditions of the compressions, intra-specimen comparisons are valid. Overall trends revealed by these analyses are important for evaluating the approximate support biomass distribution and the likely mechanical behavior of ancient plants.

5.4.3. Biomechanics and its scaling with frond parts

Our estimated mechanical and structural properties provided the first quantitative data on the variation of biomechanical features across a frond of Carboniferous age, i.e., the resistance to fracture (tensile strength), stiffness (tensile modulus of elasticity), and total resistance to bending (flexural stiffness) of pinnules and rachides of different orders. At the same time, estimated values of leaf mass per area were useful for determining the approximate degree of biomass (dry-mass) investment in structural support. In this section, density and biomechanical properties of pinnules and rachides are compared using one-way ANOVA (α = 0.05) test (Tables 11 and 12, Appendix, supplementary data) and salient results are discussed.

Mean values of density and biomechanical properties are similar amongst pinnules and rachides, although with some exceptions. In fact, pinnules and ultimate rachides were not significantly different, which is explained by the anatomical continuity of their tissues. Also, pinnules and antepenultimate rachides were not statistically different either. Results show that pinnules and antepenultimate rachides were built with organic-rich materials (i.e., higher values of C=C cont, CH_{ar}/CH_{al}, and $CH_{ar}/C=C$). However, pinnules and antepenultimate rachides invested in different types of aromatics, which included mainly resin- and tannin-bearing structures in the former and resin- and lignin-bearing compounds in the latter. Pinnules had a relatively higher metabolic cost of construction with higher contributions of sclerified tissues. Hence, they did not need to develop well-defined midveins or thickened veins since the leaf lamina provided direct mechanical support and stability (cf. Pšenička and Zodrow, 2017).

The similar and relatively high values of density, total resistance to bending, stiffness, and construction costs of pinnules and antepenultimate rachides could also be explained by the presence of secretory organs and secretory products. The latter are organic-rich compounds presumably derived from the diagenetic alteration of resin-like, phenolic-related structures. In fact, in a previous contribution we demonstrated that "the secretory organs occurred in the entire *ovata* frond, its associate petiole and trunk, and in great abundance on the pinnules" (Zodrow et al., 2016 a, b).

On the other hand, and considering pinnules and penultimate rachides, mean values of density and biomechanical properties studied were statistically higher in the former (Table 11, Appendix, supplementary data). Actually, penultimate rachides had the lowest values amongst the entire dataset with the exception of flexural stiffness (see below).

A more detailed examination of one-way ANOVA results revealed more complex trends in biomechanical properties. As observed in living plants (e.g., Niklas, 2000), under a given load and considering the total resistance to bending (flexural stiffness), larger values imply smaller amounts of energy absorbed by the plant tissue. This implies higher brittleness and subsequent smaller deformation.

Mean values of flexural stiffness for rachides of different order indicated an approximate difference of two orders of magnitude amongst them: ultimate rachis (1×10^{-5} Nm^2) < < penultimate rachis (6×10^{-3} Nm^2) < antepenultimate rachis (6×10^{-1} Nm^2). However, one-way ANOVA test (Table 11, Appendix supplementary data) indicated that flexural stiffness values of ultimate rachides, penultimate rachides, and antepenultimate rachides were not significantly different from each other. However, diameter-mean values obtained for rachides were statistically different from each other: ultimate rachis (0.001 m) < < penultimate rachis (0.004 m) < < antepenultimate rachis (0.007 m). The latter means that, although flexural stiffness values were similar amongst rachides (similar brittleness), the smallest diameters of ultimate rachides would have allowed them to break more easily than any higher order rachides. In other words, when subjected to a given stress, ultimate rachides of the *ovata* frond would have broken with a relatively lower plastic deformation absorbing a relatively smaller amounts of energy prior to fracture when compared to penultimate or antepenultimate rachides.

It seems reasonable that brittleness could have been part of the plant's ecological strategies of resistance to damage from strong winds.

Thus, higher brittleness could indicate some adaptive "self-pruning" of ultimate rachides of the *ovata* frond in strong winds during Carboniferous tropical storms. In fact, it has been suggested that coastal Variscan Foreland plains could have been subjected to monsoonal circulation (Gibling and Bird, 1994) that probably generated strong winds.

Self-pruning would have contributed to reducing drag and mechanical failure of bigger axial structures such as penultimate rachis, antepenultimate rachis, petioles, or even the main stem/trunk. This could partially explain why in the fossil record ultimate pinnae of the *ovata* plant are more frequently found than isolated pinnules, penultimate pinnae, or larger frond fragments.

5.4.4. Proximal and distal frond parts

One-way ANOVA of proximal and distal frond parts indicated, with 95% confidence, that proximal pinnules showed significantly higher contents of aromatics and higher values of density, resistance to fracture, stiffness, and construction costs than distal pinnules. It is particularly interesting to mention the notably higher mean stiffness values of proximal pinnules (2577.3 MPa), when compared to the distal ones (695.4 MPa). Accordingly, the high values of leaf mass per area of proximal pinnules (0.93 g/cm^2) are in marked contrast with that of the distal pinnules (0.75 g/cm^2) (Table 12, Appendix supplementary data). The latter is the first quantitative and statistical demonstration of the remarkably more expensive nature of proximal pinnules (see also D'Angelo and Zodrow, 2016). In other words, the *ovata* plant invested considerable amounts of resources in the construction of biomechanically resistant pinnule tissues, which were "made to last". Such chemically/mechanically reinforced structures could have been the result of higher contents of polyphenols and similar compounds allocated to and accumulated by the tissues of "older" (proximal) pinnules of the once living *ovata* plant. Additionally, this composition could have constituted a chemical defense against eventual herbivores and, most importantly, a likely nitrogen-storage mechanism developed by the *ovata* plant possibly inhabiting nitrogen-deficient, wetland soils.

Differences in the studied chemical and biomechanical features were recorded as well amongst distal and proximal rachides but they were not statistically significant, showing a continuum of variation. This makes sense because rachides played a very important role in the frond's mechanical stability, and it does not seem reasonable to expect to find major differences in mechanical properties of rachides throughout the *ovata* frond.

In the case of proximal and distal antepenultimate rachides, one-way ANOVA comparisons showed no statistical differences in the mean values of chemical composition, density, and biomechanical properties. However, and despite not being statistically different, total resistance to bending of the distal part (0.057 Nm^2) was lower than that of the proximal part (1.088 Nm^2) (Table 12, Appendix supplementary data). The latter indicates that, under a given load, proximal antepenultimate rachides absorbed little energy and deformation was minimal before fracture, if compared to distal antepenultimate rachides which were slightly more flexible. Noted is that the flexural stiffness of proximal antepenultimate rachides (1.088 Nm^2, diameter = 0.9 cm) is similar to that of the Carboniferous pteridosperm *Calamopitys* sp. (approx. 1.5 Nm^2, diameter = 4.5 cm). The latter was calculated by Rowe et al. (1993) using a very different biomechanical approach.

When proximal and distal penultimate rachides of the *ovata* frond were compared, mean values of chemical composition, density, tensile modulus of elasticity, flexural stiffness, tensile strength, and leaf mas per area were not significantly different (Table 12, Appendix supplementary data). The one-way ANOVA comparisons addressed above involved: (i) distal vs. proximal pinnules, (ii) distal vs. proximal antepenultimate rachides, and (iii) distal vs. proximal penultimate rachides. ANOVA results in the lower part of Table 12 of the Appendix (supplementary data) show the comparisons between the complete distal frond fragment vs. the complete proximal frond fragment. Complete frond fragments include data of pinnules + ultimate rachides + penultimate rachides + antepenultimate rachides. Density, tensile modulus of elasticity, tensile strength, and leaf mas per area were significantly higher in the proximal frond fragment. In fact, the basal-most part of the *ovata* frond fragment was significantly denser, much stiffer, with a higher resistance to fracture, and a higher metabolic cost of tissue construction than the distal frond part.

5.4.5. Comparisons with literature data

To the best of our knowledge, data of mechanical properties of fossil leaves are rare. Density and tensile modulus of elasticity were recorded for compression-preserved specimens of *Dicroidium dutoitii* (Corytospermales, Corystospermaceae) from the early Late Triassic of the Allan Hills, southern Victoria Land, Antarctica (Boucher et al., 1999). However, noted is that these authors estimated the mechanical properties *"using empirically measured values of living plants, and quantitative estimates of plant tissue composition from the anatomy of rachis and petioles"*.

Also, anatomical data were obtained from permineralized specimens of another taxon, i.e., *Dicroidium fremowensis*. Boucher et al. (1999) assigned separate mechanical properties to the laminar and rachial regions of *D. dutoitii*. In the laminar region density = 0.7 g/cm^3 and tensile modulus of elasticity = 150 MPa. However, in the rachial region density = 1.0 g/cm^3, and tensile modulus of elasticity = 8500 MPa. Unfortunately, tensile strength, flexural stiffness, and leaf mas per area were not recorded for *D. dutoitii*, thus precluding comparisons with our data.

Considering that density and tensile modulus of elasticity of both the *ovata* and the *dutoitii* fronds were obtained using very different approaches, and assuming that both fronds were preserved under similar (milder) physical-chemical conditions, comparisons of foliage mechanical properties could be possible. In that case, it can be argued that the density of the laminar region estimated for *D. dutoitii* (0.7 g/cm^3) is similar to density mean values obtained for pinnules of the *ovata* frond (1.09 g/cm^3). The density of the rachial region assigned to *D. dutoitii* (1 g/cm^3) is strikingly similar to density mean values obtained for ultimate rachides of the *ovata* frond (0.99 g/cm^3).

The estimated value of the tensile modulus of elasticity for the laminar region of *D. dutoitii* (150 MPa) is very low in comparison with mean values of tensile modulus of elasticity obtained for pinnules of the *ovata* frond (1550.8 MPa). In contrast, the estimated value of tensile modulus of elasticity for the rachial region of *D. dutoitii* (8500 MPa) is very high, when compared to the *ovata* frond. Values for the latter are ultimate rachides = 694.5 MPa; penultimate rachides = 575.8 MPa; antepenultimate rachides = 1821.5 MPa (Table 2).

Similarities in density values mentioned above for rachides and pinnules of both taxa likely suggest a similar chemical composition. This implies similarities in some anatomical/ physiological characteristics possibly shared by Carboniferous and Triassic seed ferns, e.g., the presence of secretory organs (resinous cells). However, the extremely large tensile modulus of elasticity value recorded for the rachial region of *D. dutoitii* could conceivably be the result of anatomical features present in the corystosperm taxon. Likely involved are transfusion tracheids, fibers within vascular bundles, and fiber-like vascular bundle sheaths, which are not typical of Paleozoic seed ferns (Pigg, 1990). Those anatomical traits perhaps included an increased content of sclerified (lignified) tissues in the rachial region of *D. dutoitii*. Likely implied is an aromatic-rich chemical composition useful for the development of support structures in the rachial regions of *D. dutoitii*, which were much stiffer than rachides of the *ovata* frond. A better understanding of the biomechanical properties and of the physiological traits is possible only after a proper chemometric analysis of the functional groups from compressions of *D. dutoitii*.

6. Discussion

The basic idea, novelty, and results of this study all rest on the

fortuitous collection of the well-preserved, largest-known (650 mm), quadripinnate *ovata* frond that architecturally conforms with a symmetrically overtopped frond structure. The excellent preservation in terms of the likely presence of geomacromolecules as resin-, tannin-, and lignin-derived compounds is obtained from IR information, i.e., type and relative contents of functional groups. We are most familiar with these through our many previous experiments involving medullosalean compression material.

These geomacromolecules presumably are the results of early diagenetically-modified biomacromolecules of the tissues of the once-living medullosalean fronds of Carboniferous age (Berner, 1980, Fig. 4.3). The four-time division of axes of the large segment of the *ovata* frond clearly provided the opportunity to track the 3D changes of these compounds. Principal component loadings together with the scarce data available from literature were used to infer likely combinations of functional groups, which were closely associated with different frond parts in 3D component space. More significantly, using a group-contribution method, density values could be calculated for the suggested chemical moieties. The inference that 3D variations of density (and concomitantly chemical moieties) were consistently associated with individual frond parts, formed the basis for the orderly interpretation of the biomechanical attributes and their interrelationships of the successive axes and pinnules. In particular, the presence of different geomacromolecules characterizing antepenultimate, penultimate, and ultimate rachides, and also pinnules from proximal and distal parts reflected frond morphology through chemical structures. This becomes clear considering the usual measures of relative distributions of aliphatic compounds and aromaticity that as a first approximation appear to be not only inversely related, or negatively correlated, but also dependent on the relatively proximal and distal frond positions. Noted is that, in general, the pinnules have a relatively lower content of aliphatics with shorter polymethylenic side chains, and higher contents of aromatics than the rachides. The summarized aromatic order is as follows: pinnule ≈ antepenultimate rachis > penultimate rachis > ultimate rachis. This translates, in conjunction with density applications, into the robustness of the antepenultimate rachial structures which had mechanical support functions of which sclerenchymous rodlets were a visible part (Zodrow and Mastalerz, 2017).

Fig. 6 is a generalized 3D model showing inferred distributions of density and associated biomechanical properties of the *ovata* frond. Here, relatively higher densities, implying higher metabolic costs of tissue construction, characterized the proximal and central parts of the antepenultimate rachides and pinnules (darker colors). In contrast, lower density values were calculated for the more flexible, distal, antepenultimate rachides and peripheral frond parts, i.e., penultimate rachides and ultimate rachides, which included their pinnules (lighter colors). Thus, the picture that emerges is that of a frond construction with the capacity to survive strong weather conditions, not unlike that seen in extant palm trees that resisted uprooting and damage with minimal loss of leaves.

Our results have a number of implications the least of which is further research in the budding science of fossil biomechanics, which includes comparisons between the *ovata* frond and other medullosalean taxa in terms of mechanical/structural properties of tissue construction materials (D'Angelo and Zodrow, 2018a). Instructive would also be a comparison with the larger ferny fronds, as for example *Acitheca* Schimper (Zodrow et al., 2006).

Another implication is in the field of reconstructive medullosalean frond methodology that presently relies heavily on assembly of fragmentary material whose contiguity is not always certain, but is projected into a frond structure. This subjective procedure can only be validated by collecting larger and larger intact specimens that, as every collector knows, is very difficult. This contrasts with the theoretical approach advocated that allows analytical testing.

Hand in hand with reconstructive methodology is considering the *ovata* frond a natural species as an additional descriptor of the life habit, in contrast with basing a species concept on ultimate pinnae or possibly larger specimens. The idea of a natural species can probably be traced back to Brongniart (1828).

Other implications/applications of our 3D density model are in the field of paleoecophysiology, supplying novel criteria that can be used to infer and reconstruct some ecological processes of individual species (autecology, this study) and of the plant community (synecology, e.g., D'Angelo and Zodrow, 2018a). As an example, our methodology could supply more information on the ability of *Linopteris obliqua* or *Macroneuropteris scheuchzeri* to seasonally shed pinnules (deciduousness; see Bell, 1938; Zodrow et al., 2007), thus illuminating a different aspect of frond construction to enrich palaeoecological understanding of medullosalean seed ferns.

Moreover, our results have profound implications for the study of the growth and development of medullosalean plants. Similar to living plants, and assuming development and growth from meristematic regions, large medullosalean fronds can provide an almost continuous ontogenetic record. Our comparative results between distal and proximal frond segments are interpreted as reflecting differences in two interrelated issues (i) frond architecture and (ii) frond ontogeny, since distal parts of the frond represent the youngest tissues. Consequently, our results dictate caution when morphology alone is used to determine the developmental stages of fragmentary, fossil-frond specimens. The same *caveats* apply to the estimation of the likely pinnatifid segmentation processes (Asama, 1960), used to draw conclusions on the evolution of the frond shape (e.g., Laveine et al., 1977).

As expected, our proposed methodology for the calculation of density and derived biomechanical properties has limitations. Chemical-structural changes produced during fossilization modify both density and related mechanical properties of the original plant materials. Labile compounds of biological origin, e.g., proteins, nucleic acids, lipids, and carbohydrates, are rarely preserved in the fossil record. The chemically most resistant and frequently found constituents of compression-preserved plants are those derived from structural compounds of resins and lignins (e.g., van Bergen et al., 2004; Zodrow et al., 2009, 2016b; D'Angelo et al., 2011; D'Angelo and Zodrow, 2018c).

The rank of coal associated with the fossils (deduced from random vitrinite-reflectance percentage, R_o%) is usually employed as an indicator of geothermal alterations, i.e., fossilization conditions. The boundary between high and medium volatile bituminous coals, at an approximate R_o% value of 1.1, signals relatively "mild" geochemical conditions, permitting the preservation of compressions with minimal chemical alteration (see D'Angelo et al., 2012 and Zodrow et al., 2009). At this juncture, it can be stated that an approximate maximum R_o% value of 1.1 indicates the limit of applicability of our methodology. Below this value compressions are relatively well-preserved, as is the case of the *ovata* frond from the Point Aconi Seam where the R_o% = 0.79%. As shown by Table 1, values of tensile modulus of elasticity recorded for some antepenultimate rachides, e.g., *24APUr*; TME = 2577.3 MPa, are remarkably similar to those reported for wood lignins (i.e., TME = 2500 to 3700 MPa; see Gibson, 2012). Those data strongly suggest that little chemical changes took place during fossilization of the most robust, structural unit of the frond, i.e., the antepenultimate rachis.

Caution is advised when working with pinnules preserved as fossilized-cuticles, because they have suffered chemical alterations which, in turn, may considerably alter the values of density and biomechanical properties. As an example, Table 1 shows considerably lower values of tensile strength of *22APUr* (3.35 MPa; preserved as fossilized-cuticle) if compared to *26APUr* (7.26 MPa, preserved as compression). Cuticles obtained in the laboratory from compressions by oxidation or other treatments require a different 3D density model since the elimination of mesophyll-derived compounds considerably changed the type and contents of functional groups. As an example, infrared peaks (at 900–700 cm^{-1}) assigned to C—H out-of-plane bending in aromatic

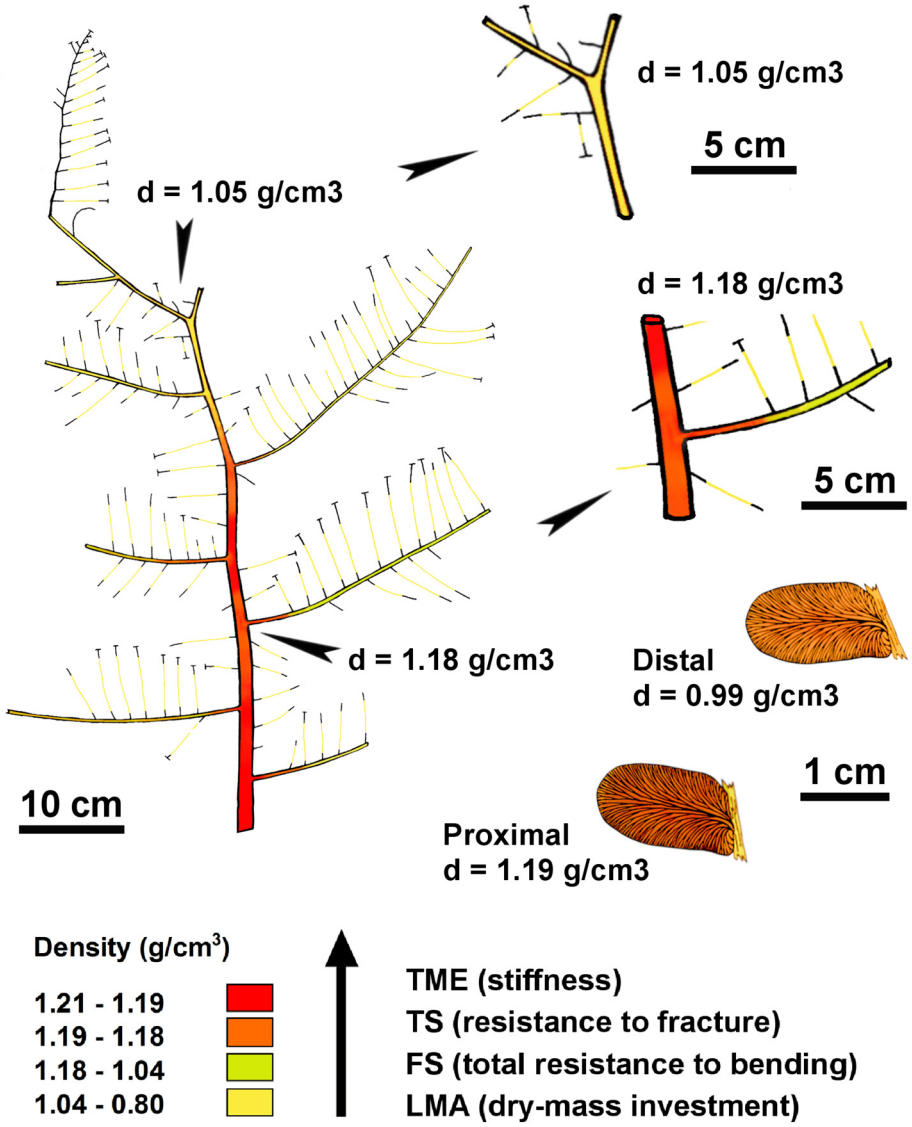

Fig. 6. Color-shaded 3D model showing density distribution and the corresponding biomechanical properties of the frond. Selected forking zones of the frond are shown in detail on the right hand of the figure. Note the darker color of proximal pinnules indicating their significantly higher values of density and biomechanical traits. Color scale is simplified from Fig. 4. See the web version of this article for a better interpretation of colors in this figure.

hydrocarbons are usually absent in cuticles (e.g., Zodrow and Mastalerz, 2002), i.e., CH_{ar} / CH_{al} ratio cannot be calculated and Eq. (1) cannot be used.

7. Concluding remarks

Illustrated in a comprehensive way is that infrared analysis of functional groups is capable of tracking chemical signatures throughout a fossil frond by means of chemometric analysis. This approach opens up new possibilities for taxonomic, systematic, physiological, and ecological studies of Carboniferous seed ferns, and possibly marattialean ferns.

Results arrived at indicate that a considerable amount of resources would have been invested by the once living *ovata* plant for the construction of metabolically expensive pinnules and rachial tissues. Such hard, tough, and resistant tissues could indicate that pinnules and rachides were "made to last" and guaranteed the biomechanical stability of the entire frond/plant, which was quite large. Furthermore, the high dry-mass investment (leaf mass per area) of pinnules and rachial tissues could be indicative of slow photosynthetic returns on investments of carbon and nutrients, probably sustained for long periods (i.e., long lifespan for leaves).

The 3D, chemistry-based model of the *ovata* frond described has provided new insights into the hitherto unknown biomechanics of this iconic medullosalean plant, which inhabited Pennsylvanian wetland landscapes. Through the novel application of chemical group-distribution to derive density estimates from the functional groups, a new theoretical research avenue has been outlined. This approach allows analysis, prediction, reconstruction, and evaluation of models that otherwise have been based solely on macroscopic and microscopic morphological observations, including fragmentary remains, not in organic attachment.

As demonstrated, our new methodology is applicable to relatively well-preserved compressions (with an approximate, maximum R_o% value of 1.1) of different vegetative plant parts and reproductive structures. The latter includes the determination of the most probable position of ovular attachment to the medullosalean frond, and the likely biomechanical properties of different layers of *Trigonocarpus grandis* (Pennsylvanian, Sydney Coalfield, Nova Scotia). This certainly could provide new insights in the mechanisms of endosperm weakening and the germination process of pteridosperms (D'Angelo and Zodrow, 2018b). Encouraging results derived from our chemometric models

present a new research field to contribute to the knowledge of extinct plants and ecosystems in a detailed and unprecedented way.

Acknowledgements

Partial financial support by Universidad Nacional de Cuyo (SCTyP N° 06/M088 – J.A. D'Angelo) is gratefully acknowledged. We cordially thank, and are much indebted to Dr. DiMichele and two anonymous reviewers for their time and efforts. Their comments, questions, and suggestions greatly contributed to improve the contents of this contribution.

Appendix A. Supplementary data

Supplementary data to this article can be found online at https://doi.org/10.1016/j.coal.2018.09.003.

References

ACD/ChemSketch, Inc, 2010. Advanced Chemistry Development, Inc. Freeware version 12.01. www.acdlabs.com (Accessed on: Jan. 15th, 2018).
Asama, K., 1960. Evolution of the Leaf Forms Through the Ages Explained by the Successive Retardation and Neoteny, 2nd Ser. (Geol.). 4. Sci. Rept. Tohoku Univ., Sendai, Japan, pp. 252–280.
Atieg, A., Watson, G.A., 2003. A class of methods for fitting a curve or surface to data by minimizing the sum of squares of orthogonal distances. J. Comput. Appl. Math. 158, 277–296.
Balsamo, R.A., Vander Willigen, C., Bauer, A.M., Farrant, J., 2006. Drought tolerance of selected *Eragrostis* species correlates with leaf tensile properties. Ann. Bot. 97, 985–991.
Barthélémy, D., Caraglio, Y., 2007. Plant architecture: A dynamic, multilevel and comprehensive approach to plant form, structure and ontogeny. Ann. Bot. 99, 375–407.
Bazzaz, F.A., Grace, J., 1997. Plant Resource Allocation. Academic Press, California (303 pp.).
Beeler, H.E., 1983. Anatomy and frond architecture of *Neuropteris ovata* and *N. scheuchzeri* from the Upper Pennsylvanian of the Appalachian Basin. Can. J. Bot. 61, 2352–2368.
Bell, W.A., 1938. Fossil Flora of Sydney Coalfield, Nova Scotia. Geol. Surv. Can. Mem. 215 (334 pp).
van Bergen, P.F., Blokker, P., Collinson, M.E., Sinninghe Damsté, J.S., de Leeuw, J.W., 2004. Structural biomocromolecules in plants: what can be learnt from the fossil record? In: Hemsley, A.R., Poole, A.I. (Eds.), The Evolution of Plant Physiology. Elsevier Academy Press, Oxford, pp. 133–154.
Berner, R.A., 1980. Early Diagenesis: A Theoretical Approach. Princeton University Press, Princeton, N.J. (241 pp.).
Bertrand, P., 1930. Bassin houiller de la Saar et de la Lorraine. I. Flore fossile. 1. Neuroptéridées. Études Gîtes Minéraux, Paris (58 pp.).
Boucher, L., Taylor, E., Taylor, T., 1999. In: Kurmann, M.H., Hemsley, A.R. (Eds.), Biomechanical stability of *Dicroidium* pteridosperm foliage. The Evolution of Plant Architecture, Royal Botanic Gardens, Kew, pp. 423–435.
Boudaoud, A., 2010. An introduction to the mechanics of morphogenesis for plant biologists. Trends Plant Sci. 15, 353–360.
Brongniart, A., 1828. In: Dufour, Chez G., D'Ocagne (Eds.), Histoire des Végétaux fossils, ou recherches botaniques et géologiques sur les végétaux renfermés dans les diverses couches du globe. Libraires-Éditeurs, Paris (288 pp.).
Constantinou, L., Gani, R., 1994. New group contribution method for estimating properties of pure compounds. AICHE J. 40, 1697–1710.
D'Angelo, J.A., Zodrow, E.L., 2011. Chemometric study of functional groups in different layers of *Trigonocarpus grandis* ovules (Pennsylvanian seed fern, Canada). Org. Geochem. 42, 1039–1054.
D'Angelo, J.A., Zodrow, E.L., 2015. Chemometric study of structural groups in medullosalean foliage (Carboniferous, fossil Lagerstätte, Canada): Chemotaxonomic implications. Int. J. Coal Geol. 138, 42–54.
D'Angelo, J.A., Zodrow, E.L., 2016. 3D chemical map and a theoretical life model for *Neuropteris ovata* var. *simonii* (index fossil, Asturian, Late Pennsylvanian, Canada). Int. J. Coal Geol. 153, 12–27.
D'Angelo, J.A., Zodrow, E.L., 2018a. Biomechanical properties of *Neuropteris ovata* and *Alethopteris ambigua* (Pennsylvanian, Canada). A chemometric approach. (MS).
D'Angelo, J.A., Zodrow, E.L., 2018b. Attachment Position and Biomechanics of Trigonocarpalean Ovules in in Medullosalean Fronds (Pennsylvanian, Canada). A chemometric approach. (MS).
D'Angelo, J.A., Zodrow, E.L., 2018c. Fossil cutin of *Johnstonia coriacea* (Corystospermaceae, Upper Triassic, Cacheuta, Argentina). Int. J. Coal Geol. 189, 70–74.
D'Angelo, J.A., Escudero, L.B., Volkheimer, W., Zodrow, E.L., 2011. Chemometric analysis of functional groups in fossil remains of the *Dicroidium* flora (Cacheuta, Mendoza, Argentina): implications for kerogen formation. Int. J. Coal Geol. 87, 97–111.
D'Angelo, J.A., Zodrow, E.L., Mastalerz, M., 2012. Compression map, functional groups and fossilization: A chemometric approach (Pennsylvanian neuropteroid foliage, Canada). Int. J. Coal Geol. 90-91, 149–155.
Donaldson, T.S., 1966. Power of the F-test for nonnormal distributions and unequal error variances. In: United States Air Force Project RAND. Memorandum RM-5072-PR.
Evert, R.F., 2006. Esau's Plant Anatomy: Meristems, Cells, and Tissues of the Plant Body: their Structure, Function, and Development, 3rd ed. John Wiley & Sons, Inc., Hoboken, New Jersey (601 pp.).
Fisher, R.A., 1970. Statistical Methods for Research Workers, 14th ed. Oliver & Boyd, Edinburgh, London (362 pp.).
Gibling, M.R., Bird, D.J., 1994. Late Carboniferous cyclothems and alluvial palaeovalleys in the Sydney Basin, Nova Scotia. Geol. Soc. Am. Bull. 106, 105–117.
Gibson, L.J., 2012. The hierarchical structure and mechanics of plant materials. J. Roy. Soc. Interface 1–18. https://doi.org/10.1098/rsif.2012.0341.
Hallé, F., Oldeman, R.A.A., 1970. Essai Sur L'architecture et la Dynamique de Croissance des Arbres Tropicaux. Masson & Cie, Paris (178 pp.).
Hatcher, P.G., 1990. Chemical structural models for coalified wood (vitrinite) in low rank coal. Org. Geochem. 16, 959–968.
Heitner, C., Dimmel, D., Schmidt, J.A., 2010. Lignin and Lignans: Advances in Chemistry. CRC Press, Taylor & Francis Group, Florida (629 pp.).
Heredia-Guerrero, J.A., Benitez, J.J., Dominguez, E., Bayer, I.S., Cingolani, R., Athanassiou, A., Heredia, A., 2014. Infrared and Raman spectroscopic features of plant cuticles: a review. Front. Pl. Sci. 5, 1–14 (Article 305).
Hoffmann, F., 1826. Über die Pflanzenreste des Kohlengebirges von Ibbenbühren und vom Piesberge bei Osnabrück, pp. 151–168, figs. 1–10. In: Keferstein, C. (Ed.), Teutschland, Geonostisch-geologisch Dargestellt, mit Charten und Durchschnittszeichungen, Welche Einen Geognostischen Altas Bilden. 4 pt.2.
Izenman, A.J., 2008. Modern Multivariate Statistical Techniques: Regression, Classification, and Manifold Learning (Springer Texts in Statistics), first ed. Springer (734 pp.).
Jankowski, M.D., Henry, C.S., Broadbelt, L.J., Hatzimanikatis, V., 2008. Group contribution method for thermodynamic analysis of complex metabolic networks. Biophys. J. 95, 1487–1499.
Laveine, J.-P., 1986. The size of the frond in the genus *Alethopteris* Sternberg (Pteridospermopsida, Carboniferous). Geobios 19, 49–56.
Laveine, J.-P., Belhis, A., 2007. Frond architecture of the seed-fern *Macroneuropteris scheuchzeri*, based on Pennsylvanian specimens from the Northern France coal field. Palaeontogr. Abt. B 277, 1–41.
Laveine, J.-P., Coquel, R., Loboziak, S., 1977. Phylogénie générale des Calliptéridiacées (Pteridospermopsida). Geobios 10, 757–847.
Masselter, T., Rowe, N.P., Speck, T., 2007. Biomechanical reconstruction of the carboniferous seed fern *Lyginopteris oldhamia*: Implications for growth form reconstruction and habit. Int. J. Plant Sc. 168, 1177–1189.
McLain, D.H., 1974. Drawing contours from arbitrary data points. Comput. J. 17, 318–324.
Méndez-Alonzo, R., Ewers, F.W., Sack, L., 2013. Ecological variation in leaf biomechanics and its scaling with tissue structure across three mediterranean-climate plant communities. Funct. Ecol. 27, 544–554.
Niklas, K.J., 1992. Plant Biomechanics: An Engineering Approach to Plant Form and Function. University of Chicago Press, Chicago (622 pp.).
Niklas, K.J., 2000. Computing factors of safety against wind-induced tree stem damage. J. Exp. Bot. 51, 797–806.
Niklas, K.J., 2004. The cell walls that bind the tree of life. Bioscience 54, 831–841.
Niklas, K.J., Kutschera, U., 2009. The evolutionary development of plant body plans. Funct. Pl. Biol. 36, 682–695.
Niklas, K.J., Spatz, H.-C., 2010. Worldwide correlations of mechanical properties and green wood density. Am. J. Bot. 97, 1587–1594.
Onoda, Y., Westoby, M., Adler, P.B., Choong, A.M.F., Clissold, F.J., Cornelissen, J.H.C., Diaz, S., Dominy, N.J., Onoda, Y., Westoby, M., Adler, P.B., Choong, A.M.F., Clissold, F.J., Cornelissen, J.H.C., Diaz, S., Dominy, N.J., Elgart, A., Enrico, L., Fine, P.V.A., Howard, J.J., Jalili, A., Kitajima, K., Kurokawa, H., McArthur, C., Lucas, P.W., Markesteijn, L., Perez-Harguindeguy, N., Poorter, L., Richards, L., Santiago, L.S., Sosinski, E.E., Van Bael, S.A., Warton, D.I., Wright, I.J., Wright, S.J., Yamashita, N., 2011. Global patterns of leaf mechanical properties. Ecol. Lett. 14, 301–312.
Petersen, H.I., Rosenberg, P., Nytoft, H.P., 2008. Oxygen groups in coals and alginite-rich kerogen revisited. Int. J. Coal Geol. 74, 93–113.
Pfefferkorn, H.W., Gillespie, W.H., Resnick, D.A., Scheihing, M.H., 1984. Reconstruction and architecture of medullosan pteridosperms (Pennsylvanian). Mosasaur 2, 1–8.
Pigg, K.B., 1990. Anatomically preserved *Dicroidium* foliage from the central Transantarctic Mountains. Rev. Palaeobot. Palynol. 66, 129–145.
Pšenička, J., Zodrow, E.L., 2017. Cuticles from Pennsylvanian marattialean fern "*Pecopteris*" *polypodioides* (C. Presl in Sternberg) Němejc from Pilsen Basin (Czech Republic) and Sydney Coalfield, (Canada). Folia 51, 13–22.
Rex, G.M., Chaloner, W.G., 1983. The experimental formation of plant compression fossils. Palaeontology 26, 231–252.
Rowe, N.P., Speck, T., Galtier, J., 1993. Biomechanical analysis of a Palaeozoic gymnosperm stem. Proc. R. Soc. Lond. 252, 19–28.
Shinn, J.H., 1984. From coal to single-stage and two-stage products: a reactive model of coal structure. Fuel 63, 1187–1196.
Viana, M., Jouannin, P., Pontier, C., Chulia, D., 2002. About pycnometric density measurements. Talanta 57, 583–593.
Vogel, S., 2003. Comparative Biomechanics: Life's Physical World. Princeton, NJ: Princeton University Press, New Jersey (582 pp.).
Wilson, J.P., 2013. Modeling 400 million years of plant hydraulics. Paleontol. Soc. Pap. 19, 175–194.
Wilson, J.P., Knoll, A.H., Holbrook, N.M., Marshall, C.R., 2008. Modeling fluid flow in *Medullosa*, and anatomically unusual Carboniferous seed plant. Paleobiology 34, 472–493.
Wilson, J.P., White, J.D., DiMichele, W.A., Hren, M.T., Poulsen, C.J., McElwain, J.C., Montañez, I.P., 2015. Reconstructing extinct plant water use for understanding

vegetation-climate feedbacks: methods, synthesis, and a case study using the Paleozoic-era medullosan seed ferns. Paleontol. Soc. Pap. 21, 167–195.
Wilson, J.P., Montañez, I.P., White, J.D., DiMichele, W.A., McElwain, J.C., Poulsen, C.J., Hren, M.T., 2017. Dynamic Carboniferous tropical forests: new views of plant function and potential for physiological forcing of climate. New Phytol. 215, 1333–1353.
Wnuk, C., Pfefferkorn, W.H., 1984. The life habits and paleoecology of Middle Pennsylvanian medullosan pteridosperms based on an in situ assemblage from the Bernice Basin (Sullivan County, Pennsylvania, U.S.A.). Rev. Palaeobot. Palynol. 41, 329–351.
Wright, I.J., Reich, P.B., Westoby, M., Ackerly, D.D., Baruch, Z., Bongers, F., Cavender-Bares, J., Chapin, T., Cornelissen, J.H.C., Diemer, M., Flexas, J., Garnier, E., Groom, P.K., Gulias, J., Hikosaka, K., Lamont, B.B., Lee, T., Lee, W., Lusk, C., Midgley, J.J., Navas, M.L., Niinemets, U., Oleksyn, J., Osada, N., Poorter, H., Poot, P., Prior, L., Pyankov, V.I., Roumet, C., Thomas, S.C., Tjoelker, M.G., Veneklaas, E.J., Villar, R., 2004. The worldwide leaf economics spectrum. Nature 428, 821–827.
Zhou, T., Han, D., 2008. A weighted least squares method for scattered data fitting. J. Comput. Appl. Math. 217, 56–63.
Zodrow, E.L., Cleal, C.J., 1985. Phyto- and chronostratigraphical correlations between the late Pennsylvanian Morien Group (Sydney, Nova Scotia, Canada) and the Silesian Pennant Measures (south Wales). Can. J. Earth Sci. 22, 1465–1473.
Zodrow, E.L., Cleal, C.J., 1988. The structure of the Carboniferous pteridosperm frond *Neuropteris ovata* Hoffmann. Palaeontogr. Abt. B 208, 105–124.
Zodrow, E.L., Mastalerz, M., 2002. FTIR and py-GC-MS spectra of true-fern and seed-fern sphenopterids (Sydney Coalfield, Nova Scotia, Canada, Pennsylvanian). Int. J. Coal Geol. 51, 111–127.
Zodrow, E.L., Mastalerz, M., 2017. Rodlets from compressed medullosalean plant fossils: Chemical and morphological studies (Late Pennsylvanian Sydney Coalfield, Canada). Folia 51, 23–30.
Zodrow, E.L., Šimůnek, Z., Cleal, C.J., Bek, J., Pšenička, J., 2006. Taxonomic revision of the Palaeozoic marattialean fern *Acitheca* Schimper. Rev. Palaeobot. Palynol. 138, 239–280.
Zodrow, E.L., Tenchov, Y.G., Cleal, C.J., 2007. The arborescent *Linopteris obliqua* plant (Medullosales, Pennsylvanian). Bull. Geosci. 82, 51–84.
Zodrow, E.L., D'Angelo, J.A., Mastalerz, M., Keefe, D., 2009. Compression-cuticle of seed ferns: Insights from liquid-solid states FTIR (Late Palaeozoic-Early Mesozoic, Canada-Spain-Argentina). Int. J. Coal Geol. 79, 61–73.
Zodrow, E.L., D'Angelo, J.A., Cleal, C.J., 2016a. The *Neuropteris ovata* frond and its cyclopteroids: micromorphology-spectrochemistry-fractal taxonomy. Propositions for restructuring and taxonomy (Pennsylvanian, Canada). Bull. Geosci. 91, 669–704.
Zodrow, E.L., D'Angelo, J.A., Taylor, W.A., Catelani, T., Heredia-Guerrero, J.A., Mastalerz, M., 2016b. Secretory organs: Implications for lipoid taxonomy and kerogen formation (Seed ferns, Pennsylvanian, Canada). Int. J. Coal Geol. 167, 184–200.
Zodrow, E.L., D'Angelo, J.A., Cleal, C.J., 2017. 3D chemometric model and frond architecture of *Alethopteris ambigua*: Implications for reconstruction and taxonomy (Medullosales, Canada). Palaeontogr. Abt. B 295 (4–6), 91–133.